A setup for integral measurements of multiple scattering angular distributions by 10- to 100-keV electrons

M. N. Martins[a,*], A. A. Malafronte[a], A. R. Petri[a,1], J. M. Fernández-Varea[b,a], N. L. Maidana[a], S. F. Barros[c], V. R. Vanin[a], A. Mangiarotti[a]

[a]*Laboratório do Acelerador Linear, Instituto de Física, Universidade de São Paulo, Travessa R 187, Cidade Universitária, CEP: 05508-900, São Paulo, SP, Brazil*
[b]*Facultat de Física (FQA and ICC), Universitat de Barcelona, Diagonal 645, ES-08028 Barcelona, Catalonia, Spain*
[c]*Instituto Federal de São Paulo, Campus Itaquaquecetuba, Rua Primeiro de Maio 500, Bairro Estação, CEP: 08571-050, Itaquaquecetuba, SP, Brazil*

Abstract

A dedicated setup has been developed to study the angular distributions of electrons traversing thin films employing the low-energy beam available from the gun of the São Paulo Microtron. In this first stage, only integral measurements are possible using the fraction of the electron beam current collected in a Faraday cup and in a ring surrounding the entrance of the former. The overall normalisation is provided by measuring the beam current collected by the scattering chamber as well, thus covering the full solid angle. In this work, important construction specifications are presented. The experience gained by operating this system is also discussed regarding its critical aspects like: avoiding cross talk between the cup and the ring both at the physical and electronic levels, measurements of small charges deposited on large objects (the chamber in particular), and conditioning of the various surfaces involved. Finally, some selected results are compared to the well-known theory by Goudsmit and Saunderson with good agreement.

Keywords:
Plural scattering, multiple scattering, small charge measurement, Goudsmit–Saunderson theory

1. Introduction

Multiple scattering (MS) of charged particles is relevant in many applications of radiation physics, like the accurate simulation of energy deposition or of detector response. Electrons are important both as primary particles and as secondaries released by the interaction of photons, protons, and other ions. Despite this, experimental data are generally old, and the most recent ones, published by Ross et al. (2008), were obtained with a medical linac under poorly controlled conditions. For electrons with energies between 10 and 100 keV, the existing measurements of MS angular distributions (not to be confused with backscattering) are by Dees and Hamermesh (1943) and Cosslett and Thomas (1964). A project has been started to overcome this situation, taking full advantage of the electron beams available at the São Paulo Microtron. The first step has been the study of angle-integrated distributions for 10- to 100-keV electrons impinging on targets with mass thicknesses from $\approx 10\ \mu\mathrm{g/cm^2}$ to $\approx 2\ \mathrm{mg/cm^2}$ and atomic numbers ranging from 6 to 83.

2. Principle of the integral measurements

The principle of performing integral measurements of the electrons scattered by the atoms in the target is to collect them with some electrodes. For practical reasons, these structures remain fixed so that they always subtend the same solid angle, as seen from the beam impact point on the target, and it is not really possible to perform a detailed angular scan. In the devised setup, the electrons scattered frontally are intercepted by a Faraday cup covering the polar angles below $\Theta_{\mathrm{FC}} = 12.0(5)^\circ$. To supplement this information, a ring has been installed around the entrance of the Faraday cup to cover the angles from $\Theta_{\mathrm{R_i}} = 14.4(5)^\circ$ to $\Theta_{\mathrm{R_o}} = 23.5(5)^\circ$, see Sec. 3. The normalisation is provided by the current collected from the rest of the chamber, which is kept insulated from the beam line and the ground.

The basic measured quantities are the ratios

$$R_{\mathrm{FC}} = \frac{Q_{\mathrm{FC}}}{Q_{\mathrm{FC}} + Q_{\mathrm{R}} + Q_{\mathrm{C}}} \ , \qquad R_{\mathrm{R}} = \frac{Q_{\mathrm{R}}}{Q_{\mathrm{FC}} + Q_{\mathrm{R}} + Q_{\mathrm{C}}} \ , \qquad R_{\mathrm{C}} = \frac{Q_{\mathrm{C}}}{Q_{\mathrm{FC}} + Q_{\mathrm{R}} + Q_{\mathrm{C}}} \ , \tag{1}$$

where Q_{FC}, Q_{R}, and Q_{C} are the charges collected in the Faraday cup, the ring, and the chamber, respectively (of course during the same time interval). Note that only two of these quantities are independent since $R_{\mathrm{FC}} + R_{\mathrm{R}} + R_{\mathrm{C}} = 1$.

The ratios (1) are connected to the probability density function (PDF) $p_{\mathrm{MS}}(\Theta)$ per unit solid angle of the electrons being

*Corresponding author: Tel.: +55-11-3091-7045.
Email address: martins@if.usp.br (M. N. Martins)
[1]Current address: INFN, Sez. Milano.

scattered into a cumulative [2] polar angle Θ by the integrals

$$R_{\mathrm{FC}} = 2\pi \int_{\cos\Theta_{\mathrm{FC}}}^{+1} p_{\mathrm{MS}}(\Theta)\, \mathrm{d}(\cos\Theta) \quad ,$$
$$R_{\mathrm{R}} = 2\pi \int_{\cos\Theta_{\mathrm{R_o}}}^{\cos\Theta_{\mathrm{R_i}}} p_{\mathrm{MS}}(\Theta)\, \mathrm{d}(\cos\Theta) \quad . \tag{2}$$

Eqs. (2) are valid under two important implicit assumptions: a) the collecting structures retain all the electrons that impinge on them (this is not completely true and corrections are actually necessary, see Sec. 5) and b) secondary electrons do not have a very important role. Some attempts have been made at biasing the ring with a positive voltage in the range from few tens to hundred volts, since it is essentially an open surface from which the secondary electrons can easily escape. This should help in retaining low-energy secondary electrons. Unfortunately, the collected charge does not stabilise with increasing polarisation. We interpret this result as an indication that stray electric fields from the polarised ring may reach both the surface of the Faraday cup and the chamber. As a consequence, these structures, subject to electron bombardment, release secondary electrons that are drawn to the ring when a positive voltage is applied. Note that the mounting of the ring has been optimised considering the projective geometry with respect to the target, see Sec. 3, and not the presence of possible stray electric fields, when polarised.

Furthermore, with the described method, no energy information is available on the electrons collected by the Faraday cup, the ring, or the chamber (in principle a negative high voltage could be applied to these structures, but it would greatly exacerbate insulation problems, strongly perturbing the charge measurement, interfere with the beam behaviour and, finally, cause large transfers of secondary electrons). This problem will only be solved in the second stage of the project where a low-cost and small-size silicon PIN diode (Malafronte et al., 2021, Mangiarotti et al., 2021) will be introduced in the chamber to scan the angular distribution. Thus, at present, we have no means to confirm that, for the measured targets, most of the electrons have undergone elastic scattering alone.

3. Setup and charge collecting structures

Part of the setup, in particular the Faraday cup, was already employed in previous cross section measurements of fundamental processes (Vanin et al., 2019); here we just recall its main features. It has the shape of a truncated cone, made of graphite, with the vertex at the nominal target position, see Fig. 1. The height of the truncated cone is 195 mm and the largest internal diameter (i.e. of the closed face opposite to the target) is 200 mm. The lateral walls and the closed face are 10- and 20-mm thick, respectively. The scattering chamber has the shape of a cylinder with a diameter of 490 mm. The lateral wall is made of stainless steel whereas the upper and lower

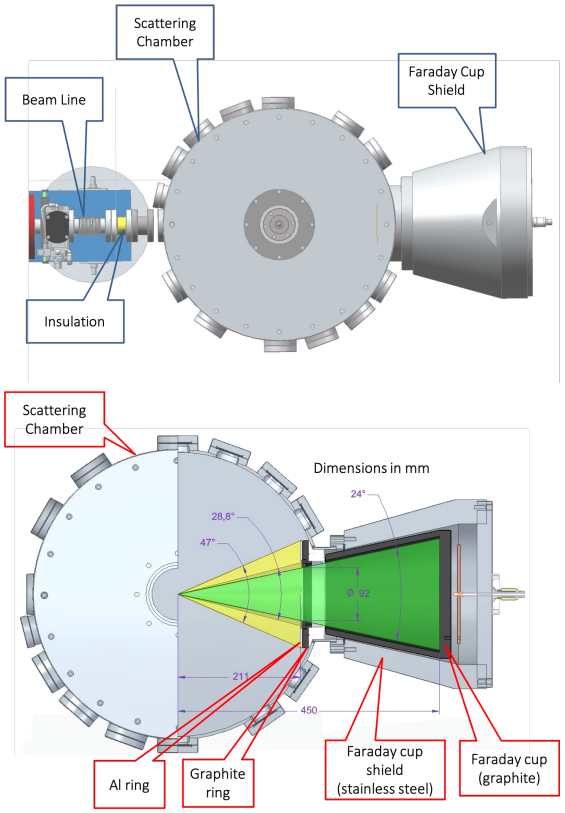

Figure 1: Technical drawings of the scattering chamber and Faraday cup: views including the final part of the beamline (upper panel) and internal structure (lower panel) are shown separately. The ring is visible in the lower panel. The values of the angles $2\,\Theta_{\mathrm{FC}}$, $2\,\Theta_{\mathrm{R_i}}$, and $2\,\Theta_{\mathrm{R_o}}$ are also indicated.

lids are aluminium plates. While in operation, the pressure inside the chamber is maintained at $\approx 7 \cdot 10^{-5}$ Pa. The Faraday cup is surrounded by a stainless steel structure, which provides both mechanical support and shielding, and is installed on the scattering chamber in the opposite position with respect to the beam entrance. To monitor any possible drift of the beam focus on the target, the Faraday cup has been supplemented with a graphite ring encircling its entrance and covering the polar angles from 12.0° to 23.1°. Moreover, the ring avoids that electrons scattered from the target can impinge on the rim of the Faraday cup. In the previous version of the setup (Vanin et al., 2019), the graphite ring was mounted on a Teflon ring that provided mechanical support, while ensuring electrical insulation. As a matter of fact, the Faraday cup retains most of the impinging electrons, scattering back into the chamber a fraction that decreases from 2% to 0.3%, when the beam energy varies from 10 to 100 keV (Vanin et al., 2019).

After several years of smooth operation, it has been discovered that the electrons backscattered by the Faraday cup reached the Teflon insulation and progressively degraded its properties. This ageing, together with the slow charging up of the Teflon surface by the same electrons, resulted in the flow of parasitic currents. The clearest evidence of this phenomenon has been manifested by measuring R_{C} in a clean situation without target and the beam directly hitting the centre of the Faraday cup.

[2] The angle Θ is the result of all multiple collisions and has to be distinguished from the deflection angle in each one.

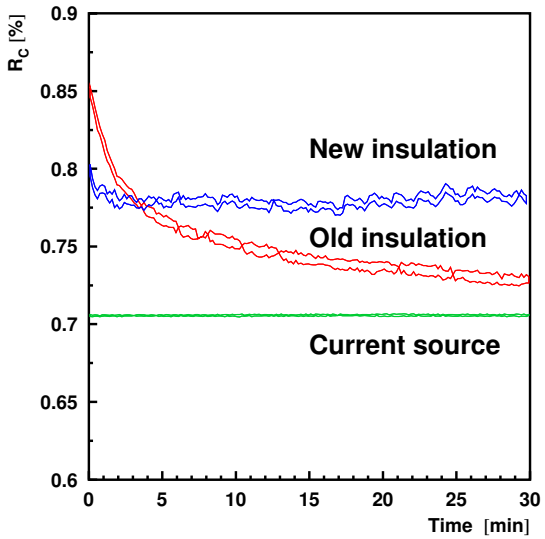

Figure 2: Ratio R_C as a function of time. Measurements with a 100-keV electron beam and no target are compared for the old and new insulations. Data obtained with no beam and a picosource, rescaled to fit on the same plot, are also displayed. The curves enclose 1 standard deviation.

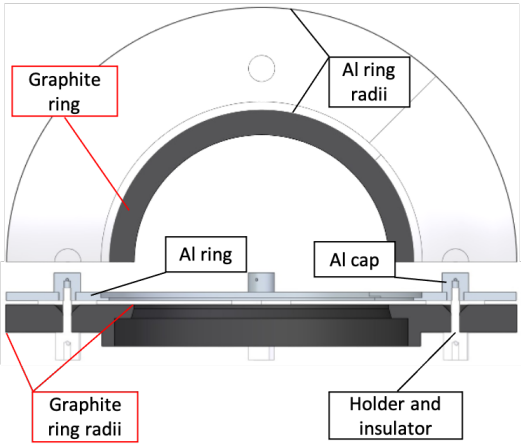

Figure 3: Top view (top) and side view (bottom) showing details of the two-ring structure. The drawing displays a cut of the system.

One such result is reported in Fig. 2 showing a time variation on the scale of about half an hour. When the beam is off, a test with a precision current source connected to the chamber (see Sec. 4), reveals no time variation indicating that the problem is induced by the electrons of the beam charging up the Teflon. A new insulation system has been designed consisting essentially of smaller Teflon rings used only around the insulating screws that support the graphite ring. In this way, the Teflon rings can hardly be reached by the beam electrons and no charge up effect is present, see again Fig. 2.

The existence of electrons that are backscattered from the Faraday cup and can hit the graphite ring from the back has another unwanted consequence: for the integral MS measurements to be correct, see Eqs. (1) and (2), the charge Q_R should be due solely to the electrons suffering deflections in the target. Therefore, it has been decided to install a second ring on top of the graphite one and insulated from it, see Fig. 3. The second ring is smaller, so that the electrons backscattered by the Faraday cup are screened by the first graphite ring, which actually covers a larger polar angle range. The dimensions of the new electrode have been chosen to avoid even electrons backscattered from the inner lateral surface of the Faraday cup to be able to reach it. The graphite ring is electrically connected to the chamber, so that the charge collected on it actually contributes to Q_C, while Q_R is the charge impinging on the second ring. The values of R_{R_i} and R_{R_o}, given in Sec. 2, already refer to the second ring.

One last issue has been studied about the second ring: its construction material. Before finalizing the choice, bulk graphite and aluminium have been irradiated by producing suitable discs that could be installed in such a way to completely close the entrance of the Faraday cup. Under this condition, R_C is actually the backscattering coefficient of the corresponding material, a quantity that must be precisely known to correct Q_R in the final measurements, see Sec. 5. The results are displayed in Fig. 4. The value of R_C is initially not constant and requires a time of the order of half an hour to stabilise. The presence of outgassing from clean metal surfaces is a well-known phenomenon (Chiggiato, 2017). The scattering chamber is baked at a temperature of ≈ 80 °C, from time to time, to maintain good vacuum. Such a process cannot be very intensive to avoid damaging the insulators (see Sec. 4) and thus it does not solve the problem of treating the surface of the ring before each measurement. Fortunately, we can rely on the conditioning at room temperature by irradiation with the electron beam itself, as shown in Fig. 4. The process was studied in detail by Scheuerlein et al. (2002) for metals, because it is of practical importance in situations where baking is impossible (e.g. for the beam pipe of the LHC). Electron stimulated desorption (ESD) of gases, mostly hydrogen, was found by Scheuerlein et al. (2002) to be the dominant process in an initial phase, followed by accumulation of carbon on the surface. The metals investigated by Scheuerlein et al. (2002) were copper and niobium, but they claim that the conclusions are somewhat general. The case of graphite is possibly different due to the peculiarities of its surface. We have preferred to fabricate the second ring with aluminium, which has a larger backscattering coefficient but stabilises faster than graphite. The choice of graphite for the Faraday cup and the first ring was actually made to minimize the emission of secondary photons, a very critical issue in other measurements, where their energy spectra are acquired (García-Alvarez et al., 2018, Barros et al., 2019, Santos et al., 2019, Barros et al., 2022b). Finally, owing to these direct observations of electron-beam conditioning, before the final MS measurements, we always let the beam impinge for half an hour on each target, without taking data, to reduce the outgassing effect on the ring and the target itself.

Due to the rather positive experience with the two-ring structure described, a similar one (but with both rings made of aluminium) has been manufactured and mounted on a movable stand. The protection electrode is always connected to

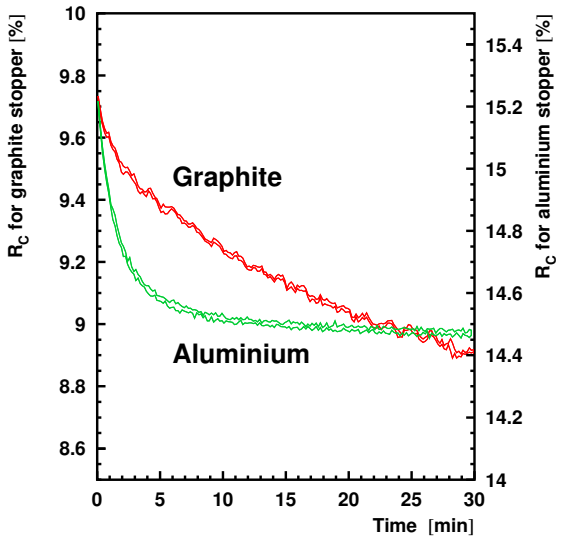

Figure 4: Ratio R_C as a function of time. Measurements with a 100-keV electron beam incident perpendicularly on graphite (left scale) and aluminium (right scale) blocks are compared. The curves enclose 1 standard deviation.

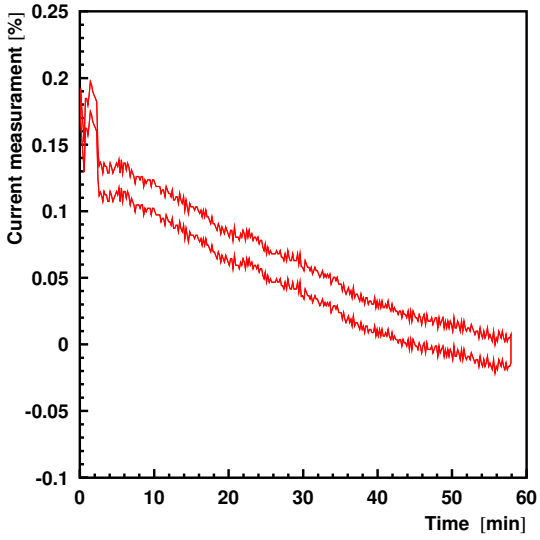

Figure 5: Current measured with one of the charge integrators as a function of time. Actually, only the percentage deviation with respect to the asymptotic value is shown to display the effect of the warm-up of the device. The curves enclose 1 standard deviation.

the chamber, allowing a unidirectional measurement of electron flow with the other. It has been used to study the background produced by the presence of the target. In particular, for the thick high-Z targets, a large fraction of the electrons is backscattered, can reach the chamber walls, and, finally, is once more backscattered with sufficient intensity to distort the measured Q_{FC} and Q_R. More details can be found in the paper dealing with these targets (Barros et al., 2022a).

4. Charge measurement

The measurement of Q_C faces the difficult task of ensuring a suitable electrical insulation of a large object with several interconnections. In particular: i) the chamber itself mechanically rests on four supports that are insulated with Teflon rings, ii) the beam line is insulated with a special vacuum-tight ceramic joint, iii) the tubing to the vacuum pump is also insulated with a special Teflon joint, and, finally, iv) all electrical connections must run through insulated feedthroughs. As discussed in Sec. 3, all insulating surfaces exposed to the beam have the potential danger of charging up. Hence, a collimator was installed inside the beam pipe before the ceramic joint in order to avoid that the electrons hit the ceramic. Using insulated feedthroughs (iv) is necessary to avoid that the charge collected by the chamber may flow through the ground of the detectors electronic chains. The target support structure, including a special linear actuator used for positioning, is electrically connected to the chamber, meaning that electrons stopped inside the target actually contribute to Q_C. The Teflon rings, ceramic joint, and Teflon joint must be periodically cleaned to avoid a deterioration of their insulation properties. By polarising the chamber to about 100 V, its resistance towards ground, in good cleaning conditions, has been measured to be ≈ 5 GΩ. Note that during normal operation, the chamber is grounded through the charge measuring circuit and its potential difference to ground never exceeds tens of mV.

The charges Q_{FC}, Q_R, and Q_C are measured with three Digital Current Integrators, model 439 by ORTEC. They are digital because they generate a logic pulse each time they collect (integrate) a (user selectable) fixed magnitude of charge (Glass et al., 1967). The integrating capacitor is actually never short circuited and the collected charge is offset by a well-controlled pulse of opposite polarity, thus avoiding any dead time (Glass et al., 1967). The pulse outputs of the three Ortec 439 modules are externally connected to a custom-made board containing three counters that are read and reset at regular time intervals of 1 s. In such a way, a time histogram of the collected charge can be built. To test the electrical properties of the system, a precision external picoampere current source, here called picosource, model 261 by Keithley has been employed. Three main tests have been undertaken.

The picosource has been connected in turn to the Faraday cup, ring, and chamber to verify that no charge is read in the other unconnected two channels. No electrical cross talk is thus present between Q_{FC}, Q_R, and Q_C.

The time stability of the Ortec 439 modules has also been studied with the picosource. In particular, the latter has been turned on for several hours before powering the former. The immediately successive charge measurements then show a small warm-up effect, visible in Fig. 5, with a time duration of about 1 h. Therefore, we always let the equipment switched on for at least 1 h before starting the actual MS measurements.

The linearity and calibration of each of the three Ortec 439 modules has been checked against the picosource. A proportionality constant (the Ortec 439 has a very special design to greatly reduce any input parasitic current (Glass et al., 1967)) has been fitted to the measured values versus the reference ones.

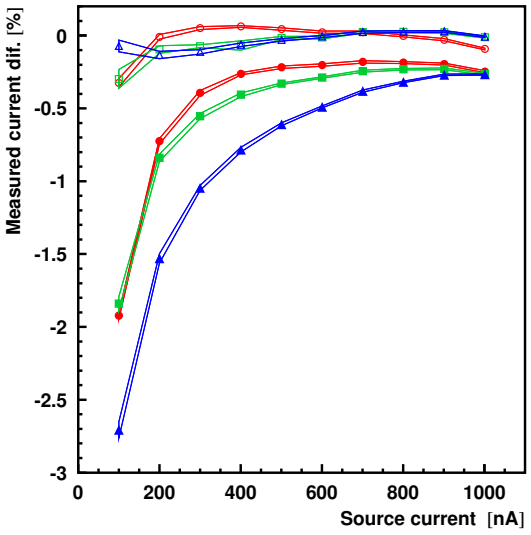

Figure 6: Percentage deviation from a linear calibration of the charge integrators performed with the picosource. The modules used for the Faraday cup (circle), the ring (square), and the chamber (triangle) are shown separately. Two cases are considered: one when the source is directly connected to the charge integrator and one when the setup is present (open and closed symbols, respectively). The curves enclose 1 standard deviation.

The percentage deviations from the straight line so determined are displayed in Fig. 6. Each Ortec 439 module (see different symbols in Fig. 6) has been tested independently. Moreover, two cases are considered: in the ideal one (open symbols in Fig. 6), the picosource is directly connected to the charge integrator with a short cable. The differences from the linear behaviour are well compatible with the stated accuracy of the Ortec 439 (0.3% for the setting of 10^{-10} Coulomb/pulse and the probed current range) and the picosource (0.25%). In a more realistic situation (closed symbols in Fig. 6), the picosource has been connected to the corresponding collecting electrode (i.e. Faraday cup, ring, or chamber) maintaining the full cable length necessary to reach the Ortec 439 modules. The proportionality constant, fitted in the previous case, has been kept to evaluate the deviations and reveal any small discrepancy in the collected charge. The conclusion is now markedly different: an ohmic loss of $\approx$ 0.5% is present for currents of 1 μA supplemented by a non-ohmic increase to $\approx$ 2% for lower ones down to 100 nA. The situation of the chamber (a large object with challenging insulation problems, see Sec. 3) is even worse, the loss reaching 3% at 100 nA.

The counts-to-charge calibration simplifies between the numerators and denominators of Eqs. (1), as long as it is permissible to assume a linear proportionality with a constant, which is the same for the three channels (thus, allowing only for equal ohmic losses). Therefore, it has been decided to use the data from Fig. 6 to separately calibrate each channel. The measured counts are thus connected to the charges appearing in Eqs. (1) by a third order polynomial, whose constant coefficient is taken to be zero.

5. Results

The setup has been employed to measure integrated MS distributions using thin non self-supporting targets deposited on C film backings (mass thicknesses from $\approx$ 5 to 20 μg/cm^2); intermediate targets (mass thicknesses from $\approx$ 100 to 300 μg/cm^2); and, finally, thick targets (mass thicknesses from $\approx$ 1.5 to 5 mg/cm^2). The results for the particular cases of the thin (with C backings) and thick (where energy loss is large) targets can only be compared with Monte Carlo simulations. More detailed accounts are being published (Barros et al., 2023, 2022a), here only the intermediate targets are discussed.

To be compared to theory, see Eqs. (2), it is necessary to apply corrections to Eqs. (1) to take into account that a small fraction $f_{\rm FC}$ of the electrons entering the Faraday cup is backscattered and can escape to the chamber (or the back of the graphite ring connected to the chamber, see Sec. 3), and a larger fraction $f_{\rm R}$ of the electrons impinging on the ring is backscattered, as well, into the chamber. Note that these corrections do not alter the denominator of Eqs. (1), which represents the total charge delivered by the beam. Therefore, the quantities $R_{\rm FC}$ and $R_{\rm R}$ in Eqs. (2) should be replaced with $F_{\rm FC}$ and $F_{\rm R}$, respectively, given by

$$\begin{aligned} F_{\rm FC} &= R_{\rm FC}\,(1 + f_{\rm FC}) \ , \\ F_{\rm R} &= R_{\rm R}\,(1 + f_{\rm R}) \ . \end{aligned} \tag{3}$$

The factor $f_{\rm FC}$ has been directly measured using hollow frames (Barros et al., 2023). The strategy has been different for $f_{\rm R}$: the electrons from the target impinge on the ring with an angle from the perpendicular direction varying between $\Theta_{\rm R_i}$ and $\Theta_{\rm R_o}$, see Fig. 1, but, unfortunately, we do not have a provision to place an aluminium plate inclined by a well-known angle in the setup. Therefore, $f_{\rm R}$ has been taken from Monte Carlo simulations performed with the PENELOPE package (Baró et al., 1995, Sempau et al., 1997, Salvat, 2015) version 2018 (Salvat, 2019) after a validation with measurements done at normal incidence (Barros et al., 2023).

To ensure good-quality data, it is necessary to check the focusing of the beam, employing hollow frames with holes of different diameters, to verify that the beam does not drift, by applying statistical tests on the constancy of $R_{\rm FC}$ and $R_{\rm R}$ during the experiment and, last but not least, to know the mass thickness of the targets accurately (Barros et al., 2023). The final results for the intermediate cases (Al 125(1), Cu 346(3), and Au 121(5) μg/cm^2) are shown in Fig. 7.

There is a clear general trend in Fig. 7: $F_{\rm FC}$ steadily increases with energy, while $F_{\rm R}$ reaches a maximum and afterwards steadily decreases. Both tendencies are the result of the MS angular distribution $p_{\rm MS}(\Theta)$ gradually evolving from a broad one to forward focused for higher electron energies. Then the electrons are more and more scattered into the Faraday cup so that $F_{\rm FC}$ tends to one. On the other hand, while $p_{\rm MS}(\Theta)$ is making the transition from being broad to forward focused, for some intermediate energies, several of the particles are deflected just into the Θ interval from $\Theta_{\rm R_i}$ to $\Theta_{\rm R_o}$ covered by the aluminium ring, resulting in a maximum of $F_{\rm R}$.

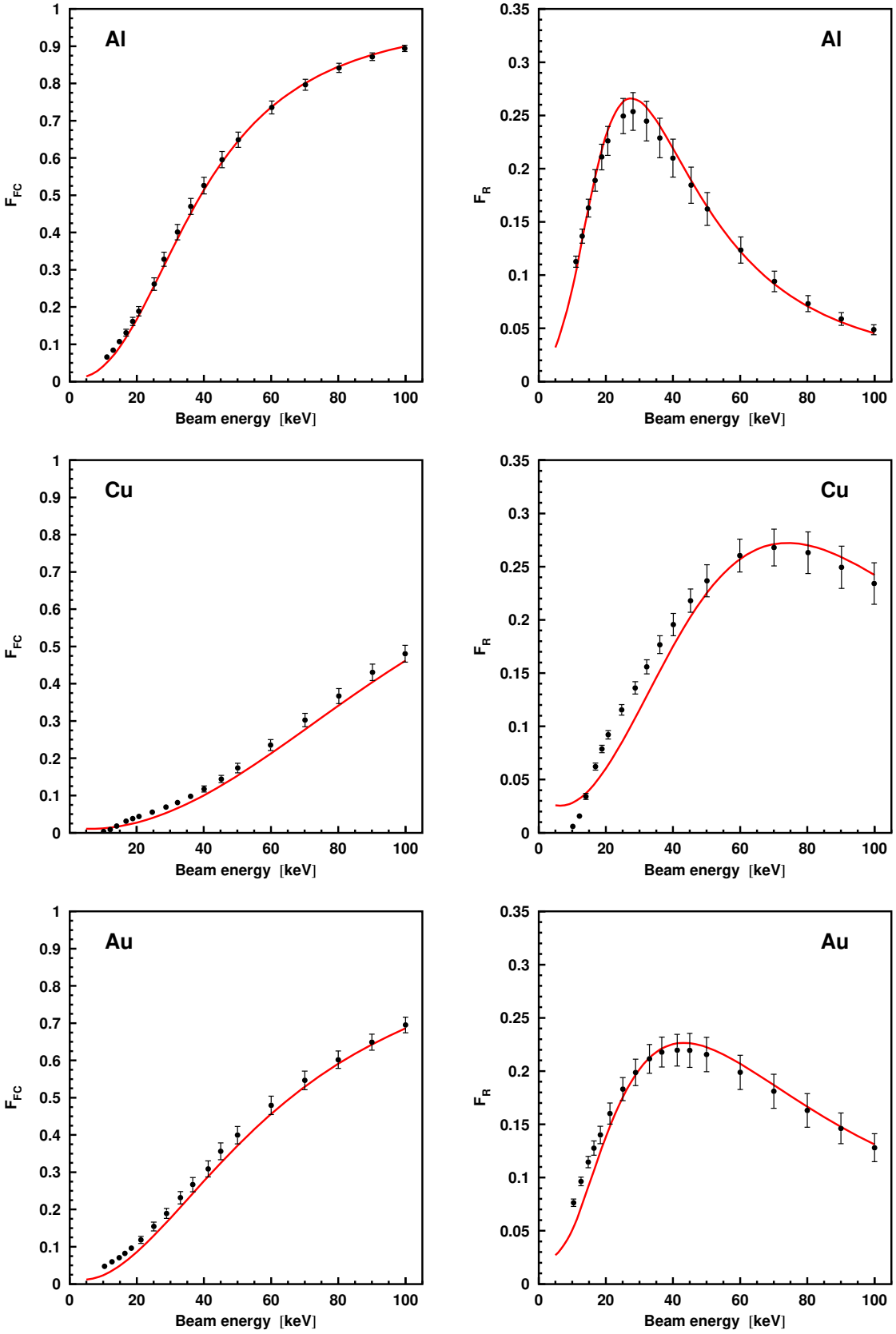

Figure 7: Measurements of F_{FC} and F_R, see Eqs. (3), as a function of the electron beam energy for the intermediate Al, Cu, and Au targets. The symbols with uncertainty bars (representing 1 standard deviation) are the data, while the curves are the predictions of the Goudsmit–Saunderson theory.

The data are compared with the theory by Goudsmit and Saunderson (1940a,b) employing the programs and the elastic differential cross section (DCS) database distributed with the ICRU Report 77 (Berger et al., 2007). The DCSs have been calculated with a partial-wave solution of the Dirac equation with a central potential which, in turn, is the outcome of a self-consistent Dirac–Fock procedure for isolated atoms. The overall agreement is quite good, despite the fractional energy loss in the target, not accounted for in the Goudsmit–Saunderson approach, which is not small for electron energies below $\approx$ 30 keV (Barros et al., 2023). This is particularly the case for the Cu target, which can fully stop 10 keV electrons, explaining the simultaneous drop in both F_{FC} and F_{R} at low energies. A target-generated background is possibly responsible for the small discrepancies relative to the Goudsmit-Saunderson calculations, seen specifically for Au at low energies in Fig. 7. Its study is presented in connection with the results for the thick targets (Barros et al., 2022a), employing the measurements with the movable two-ring structure mentioned in Sec. 3. Moreover, the role of inelastic collisions also has to be discussed (Barros et al., 2023).

6. Conclusions

A setup dedicated to integral measurements of MS angular distributions by electrons with energies between 10 and 100 keV crossing targets, made of several elements and with a wide range of mass thicknesses, has been developed. The electrons are collected with a Faraday cup, a ring mounted around it, and the scattering chamber. The first two are made of graphite. The geometry of the Faraday cup greatly reduces the fraction of electrons that are scattered back and can escape, but, since it receives a large part of the beam, especially when using thin targets, these electrons can still produce unwanted effects, like charging up exposed insulators or hit the ring from the back. The ring is supported by insulators that remain protected even of stray beams. A second ring has been installed in front of the first, which is then used as a screen and connected to the chamber. The second ring is made of aluminium: although the fraction of backscattered electrons is larger than for graphite, it takes less time to stabilise. It is also important to condition the exposed surfaces with the beam for at least half an hour before starting the actual MS measurements.

By the means described, the insulation resistance of the chamber, a large macroscopic object with several interconnections, is maintained around 5 GΩ.

The electronic system employed to measure the collected charges has been carefully characterised. A warm-up time of at least half an hour is necessary for thermal stabilisation. A calibration with a precision current source has been made to correct for the non-ohmic charge losses due to imperfections in the insulators.

Finally, a part of the full set of collected results, concerning self-supporting Al, Cu, and Au targets with mass thicknesses between $\approx$ 100 to 300 μg/cm^2, has been compared with the standard Goudsmit–Saunderson approach, finding good agreement when employing elastic DCSs from the ICRU Report 77.

7. Acknowledgements

This work has been supported by FAPESP (Fundação de Amparo à Pesquisa do Estado de São Paulo) Grant No. 2016/13116-5. A. R. P. acknowledges support by FAPESP Grant No. 2017/12661-2, J. M. F.-V. by the Spanish Ministerio de Ciencia, Innovación y Universidades, Grant No. PGC2018-096788-B-I00, and A. M. by CNPq (Conselho Nacional de Desenvolvimento Científico e Tecnológico) Grant No. 306331/2016-0 and No. 311915/2020-5.

References

Baró, J., Sempau, J., Fernández-Varea, J. M., Salvat, F., 1995. PENELOPE: An algorithm for Monte Carlo simulation of the penetration and energy loss of electrons and positrons in matter. Nucl. Instrum. Methods Phys. Res. B 100, 31.

Barros, S. F., Petri, A. R., Malafronte, A. A., Fernández-Varea, J. M., Maidana, N. L., Martins, M. N., Silva, T. F., Vanin, V. R., Mangiarotti, A., 2023. Integral measurements of plural and multiple scattering of electrons with energies between 10 and 100 keV for $6 \leq Z \leq 83$: I. Thin and intermediate targets. Radiat. Phys. Chem. 202, 110540.

Barros, S. F., Petri, A. R., Malafronte, A. A., Fernández-Varea, J. M., Maidana, N. L., Martins, M. N., Vanin, V. R., Mangiarotti, A., 2022a. Integral measurements of plural and multiple scattering of electrons with energies between 10 and 100 keV for $13 \leq Z \leq 79$: II. Thick targets. Radiat. Phys. Chem. to be published.

Barros, S. F., Vanin, V. R., Maidana, N. L., Malafronte, A. A., Fernández-Varea, J. M., Pindzola, M. S., 2022b. Experimental and theoretical L-subshell ionization cross sections for $_{83}$Bi by electron impact from the L_3 threshold to 100 keV. Phys. Rev. A 105, 012818.

Barros, S. F., Vanin, V. R., Mangiarotti, A., Maidana, N. L., Fernández-Varea, J. M., 2019. Atomic alignment of $_{73}$Ta, $_{74}$W, and $_{79}$Au after L_3 subshell ionization by 10–100-keV electron impact. Phys. Rev. A 100, 062705.

Berger, M. J., Jablonski, A., Bronić, I. K., Mitroy, J., Powell, C. J., Salvat, F., Sanche, L., 2007. Report 77: Elastic Scattering of Electrons and Positrons. Journal of the International Commission on Radiation Units and Measurements 7 Issue 2.

Chiggiato, P., 2017. Outgassing properties of vacuum materials for particle accelerators. Proceedings of the 2017 CERN–Accelerator–School, course on Vacuum for Particle Accelerators, Glumslov, Sweden.

Cosslett, V. E., Thomas, R. N., 1964. Multiple scattering of 5 - 30 keV electrons in evaporated metal films i: Total transmission and angular distribution. Brit. J. Appl. Phys. 15, 883.

Dees, B. C., Hamermesh, B., 1943. The small angle scattering of electrons by aluminum. Phys. Rev. 63, 297.

García-Alvarez, J. A., Fernández-Varea, J. M., Vanin, V. R., Maidana, N. L., 2018. Measurement of doubly differential electron bremsstrahlung cross sections at the end point (tip) for C, Al, Te, Ta and Au. J. Phys. B: At. Mol. Opt. Phys. 51, 225003.

Glass, F. M., Courtney, C. C., Kennedy, E. J., Wilson, H. N., 1967. A new approach to direct current integration. IEEE Trans. Nucl. Sci. 14, 143.

Goudsmit, S., Saunderson, J. L., 1940a. Multiple scattering of electrons. Phys. Rev. 57, 24.

Goudsmit, S., Saunderson, J. L., 1940b. Multiple scattering of electrons. II. Phys. Rev. 58, 36.

Malafronte, A. A., Petri, A. R., Gonçalves, J. A. C., Barros, S. F., Bueno, C. C., Maidana, N. L., Mangiarotti, A., Martins, M. N., Quivy, A. A., Vanin, V. R., 2021. A low-cost small-size commercial PIN photodiode: I. Electrical characterisation and low-energy photon spectrometry. Radiat. Phys. Chem. 179, 109103.

Mangiarotti, A., Petri, A. R., Malafronte, A. A., Gonçalves, J. A. C., Barros, S. F., Bueno, C. C., Fernández-Varea, J. M., Maidana, N. L., Martins, M. N., Vanin, V. R., 2021. A low-cost small-size commercial PIN photodiode: II. comparison of measurements with monoenergetic electrons to analytical expressions and Monte Carlo simulations. Radiat. Phys. Chem. 182, 109102.

Ross, C. K., McEwen, M. R., McDonald, A. F., Cojocaru, C. D., 2008. Measurement of multiple scattering of 13 and 20 MeV electrons by thin foils. Med. Phys. 35, 4121.

Salvat, F., 2015. The PENELOPE code system. Specific features and recent improvements. Annals of Nuclear Energy 82, 98.

Salvat, F., 2019. PENELOPE-2018, A Code System for Monte Carlo Simulation of Electron and Photon Transport. OECD Nuclear Energy Agency, Workshop Proceedings, Barcelona, Spain, 28 January – 1 February.

Santos, O. C. B., Vanin, V. R., Maidana, N. L., Martins, M. N., Tabacniks, M. H., Rodrigues, C. L., Silva, T. F., Santos, A. D., Barros, S. F., García-Alvarez, J. A., Koskinas, M. F., Fernández-Varea, J. M., Pindzola, M. S., 2019. Experimental and theoretical cross sections for K-shell ionization of $_{52}$Te, $_{73}$Ta, and $_{83}$Bi by electrons with energies up to 100 keV. Phys. Rev. A 100, 022703.

Scheuerlein, C., Taborelli, M., Hilleret, N., Brown, A., Baker, M. A., 2002. An AES study of the room temperature conditioning of technological metal surfaces by electron irradiation. App. Surf. Sci. 202, 57.

Sempau, J., Acosta, E., Baró, J., Fernández-Varea, J. M., Salvat, F., 1997. An algorithm for Monte Carlo simulation of coupled electron-photon transport. Nucl. Instrum. Methods Phys. Res. B 132, 377.

Vanin, V. R., Maidana, N. L., Mangiarotti, A., Lima, R. R., Malafronte, A. A., Barros, S. F., Martins, M. N., 2019. The 10 – 100 keV beam line of the São Paulo Microtron electron accelerator. Radiat. Phys. Chem. 154, 26.